MC SIMULATION OF SCATTER INTENSITIES IN A CONE-BEAM CT SYSTEM EMPLOYING A 450 kV X-RAY TUBE

A. Miceli[ab], R. Thierry[a], A. Flisch[a], U. Sennhauser[a], F. Casali[b]

[a]Empa - Swiss Federal Laboratories for Materials Testing and Research,

Electronics/Metrology Laboratory, Switzerland

[b]Università di Bologna, Department of Physics, Italy

ABSTRACT

A Monte Carlo simulation, based on GEANT4, has been developed to compute the contribution of first-order, second-order, and higher order scattering in a Computed Tomography (CT) system equipped with an industrial 450 kV X-ray tube and an area detector. The validation of simulation against the experimental data showed a good agreement. The amount of scattering produced by several hollow aluminum cylinders was simulated. It is shown that the scatter-to-primary ratio (SPR) is approximately 5 % for the aluminum cylinder of outer diameter of 75 mm, 16 % for the diameter of 100 mm, 91 % for the diameter of 150 mm, and for the diameter of 200 mm it can rise to 230 % in the regions corresponding to the maximum path length. Therefore, the scatter from the object significantly affects quantitative accuracy. Furthermore, the background scatter has been experimentally investigated. The results show that the background scatter plays an important role and has to be reduced using collimators.

KEYWORDS: Monte Carlo simulation; cone beam computed tomography; scatter

1. INTRODUCTION

The predominant interaction of photons with matter at the energies considered for NDT applications (up to 450 keV) is the Compton scattering [1]. As a consequence of the interaction, the photons lose part of their energy and they are deflected from their original path. If the scattered photons reach the detector, they result in an increase of the registered total intensity and consequently an underestimation of attenuation in each projection. This leads to cupping and streak artifacts on the reconstructed images [2-4].

Area detectors are much more affected by the scattered radiation compared to linear detectors because of the increased volume coverage. It is therefore essential, if we deal with area detectors, to evaluate the spatial distribution of the scatter signal in order to develop scatter correction algorithms and to optimize tomograph design parameters.

Monte Carlo (MC) simulations of X-ray scatter constitute an established method to provide this information [5-8]. Although extensive studies have been carried out in the medical field, in the area of CT systems for NDT application they are rather limited [9].

The aim of this paper is to study the importance of the scattering generated by the investigated object in a CT system equipped with a 450 kV X-ray tube and an area detector. For this purpose a MC simulator based on GEANT4 has been developed and validated by comparison with experimental data.

The object is not the only source of scattering in an X-ray CT system. The structure of the CT system and the walls of the X-ray room are responsible for the production of a non-negligible amount of scatter (background scatter). Experiments using different apertures of the X-ray beam were carried out to evaluate the degradation of the contrast due to the background scatter.

2. MATERIALS AND METHODS

2.1 CT scanner

All measurements have been performed using a CT system prototype designed and built in the framework of the European project DETECT (figure 1).

X-ray source. The system was provided with a 450 kV/2mA X-ray tube (COMET MXR-451) with a focal spot size of 2.5 mm. The inherent filtration of the tube was 2.3 mm Fe and 1.0 mm Cu. The angle of the tungsten target was 30°. A 1.0 mm tungsten attenuator was utilized to reduce the primary flux of low energy photons. The X-rays were collimated so that the aperture of the beam was 3.2° x 3.2° (aperture 1) in order to reduce the scatter background. The test objects were completely illuminated. To measure the degradation of the contrast the following X-ray beam apertures were considered: 5.6° x 5.6° (aperture 2), 8.9° x 6.1° (aperture 3) and 20° x 20° (aperture 4) corresponding to the uncollimated beam.

Detector. A 2 mm thick Thallium doped Cesium Iodine, CsI (Tl), scintillating screen was used to convert the X-ray radiation to visible light. The light was reflected by a 45° mirror onto a cooled CCD camera (16 bits at 1 MHz, Apogee Alta U32, 2184 x 1472 pixels each sized 6.8 x 6.8 μm^2). The mirror and the camera were placed inside a shielding box, i.e. detector box, whose walls were made of three adjacent layers of steel, lead, and steel with 3, 3, and

5 mm thickness, respectively. The source-detector distance was 1500 mm. A filter of silver was placed at 1461 mm from the source. The shielding room was 3.6 x 2.9 x 3.7 m^3.

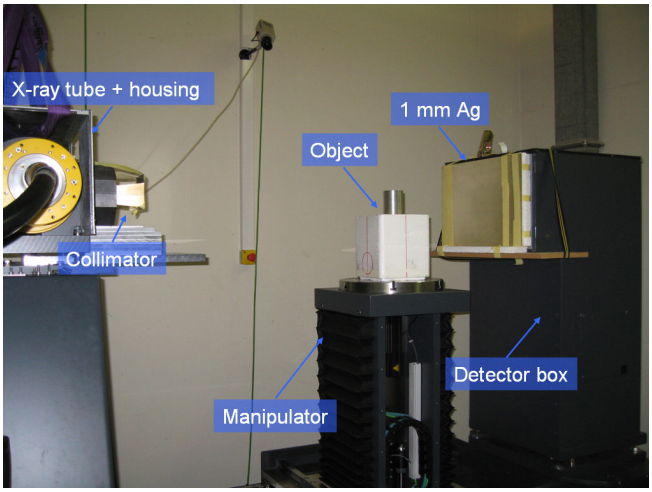

Figure 1. CT system. The X-ray tube, the source-collimator, the manipulator, the filter of silver, and the detector box are clearly visible.

2.2 Simulation

The Monte Carlo calculations were performed using the low energy extension of the particle transport simulation toolkit GEANT4 version 4 [10-12]. The electromagnetic processes taken into account were: Rayleigh scattering, Compton scattering, and photoelectric effect, for photons, ionization, bremsstrahlung, and multiple scattering, for electrons.

X-ray spectrum. The energy spectrum of the X-ray source that was used as an input to the MC simulations further discussed in this paper was simulated according to the specifications of the manufacturer using 2 x 10^9 histories. Figure 2a displays the setup of the simulation of the energy spectrum of the X-ray tube. The X-ray photons are generated by interaction of a monochromatic electron beam of 450 keV with the tungsten target. The X-ray beam is then filtered by the inherent filtration of the tube and by the external filtration of 1.0 mm thick tungsten (Figure 2b). The X-ray spectrum is retrieved within an angle of 20° with respect to the central axis of the beam. The simulated spectrum has been validated by comparison with experimental data [13].

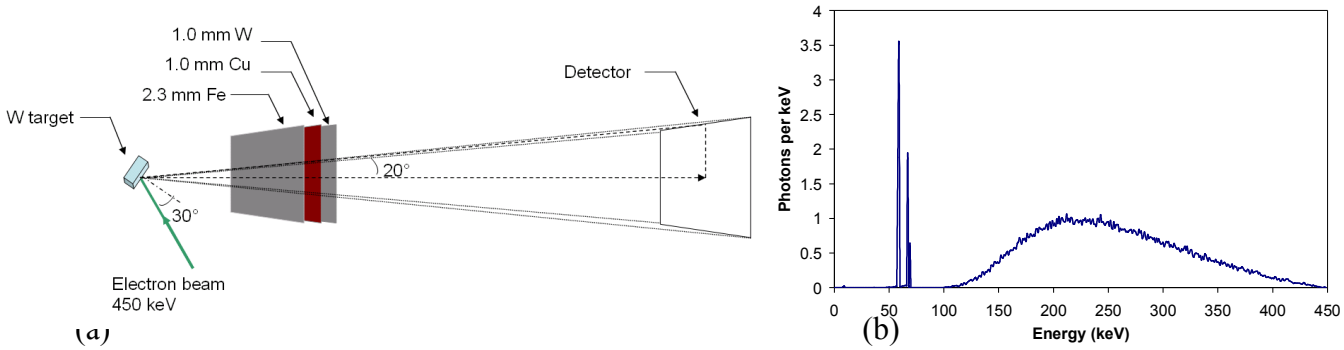

Figure 2. (a) Simulation setup used to calculate the spectrum of the X-ray source. (b) Energy spectrum of the tube at 450 kV.

Projections. The X-ray photons, whose energies are sampled randomly from the simulated spectrum, are directed towards the detector. If the photon is inside the object, it is followed along its path through the object until it leaves the volume or is absorbed. If the detector is hit, the corresponding detector pixel is determined and the energy deposited by the electrons produced within the material is stored. Before the photon reaches the detector, it interacts with the filter of silver (1.0 mm thick) and with the support of the scintillator (aluminum, 1.0 mm thick). Figure 3 shows the setup of the simulation used for the validation. The images formed by direct radiation, first-order, second-order and higher order scattered photons were retrieved. The images of the scattering were de-noised using the Richardson-Lucy algorithm [9]. The procedure utilizes a maximum likelihood algorithm to retrieve the original noise-free signal blurred by a Gaussian kernel. The number of interactions of the Richardson-Lucy fit was set to 10 and the standard deviation of the Gaussian kernel to 30 detector pixels.

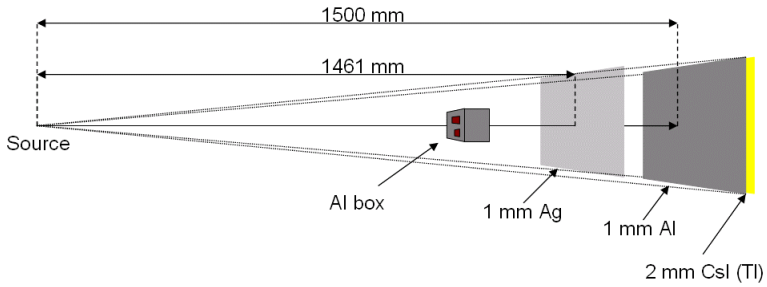

Figure 3. Setup used to simulate the radiography of a test object.

2.3 Validation of the simulation

To validate the simulation, we compared the simulated and measured radiographies of two test objects: (i) an aluminum step wedge (size: 100 x 100 x 20 mm^3; 5 steps of thickness ranging from 20 to 100 mm) and (ii) an aluminum box (size: 50 x 65 x 50 mm^3) with two copper rods along the axial direction with equal distance from the object centre of size 10 x 10 x 50 mm^3 and 8 x 10 x 50 mm^3. The measure of agreement was evaluated calculating the normalized error, NE, using the equation (1) formulated by [14]:

$$NE(u,v) = \frac{p_{Measured}(u,v) - p_{Simulation}(u,v)}{p_{Measured}(u,v)} \quad (1)$$

where u, v are the coordinates on the detector, $p_{Measured}(u,v)$ and $p_{Simulated}(u,v)$ are the measured and simulated projections.

2.4 Characterization of the scatter distribution

Hollow aluminum cylinders of various outer diameters and heights were simulated to evaluate the percentage of scattered radiation. The inner radius for all the hollow cylinders was 25 mm and their heights were 75, 100, 150, and 200 mm. The outer radius for each cylinder was half of its height.

The amount of first-order scattering was characterized in terms of the first-order scatter to primary ratio, SPR_1, defined by:

$$SPR_1(u,v) = \frac{S_1(u,v)}{P(u,v)} \quad (2)$$

the second-order scattering by SPR_2:

$$SPR_2(u,v) = \frac{S_2(u,v)}{P(u,v)} \quad (3)$$

and the higher than second order scattering by $SPR_{>2}$:

$$SPR_{>2}(u,v) = \frac{S_{>2}(u,v)}{P(u,v)} \quad (4)$$

where $S_1(u,v)$ is the detected first-order scattered radiation on the pixel of coordinates (u,v), $S_2(u,v)$ is the second-order scattered radiation, $S_{>2}(u,v)$ is the higher than second-order scattered radiation, and $P(u,v)$ is the primary radiation.

2.5 Background scatter

To quantify the degradation due to the background scatter, projections of the aluminum box without copper rods were acquired using different X-ray beam apertures (aperture 1 – aperture 4). To evaluate the degradation of the image due to the background scatter we calculated from the profiles, for each aperture, the contrast degradation factor, *DFC(n)*, given by:

$$DFC(n) = \frac{C(1)}{C(n)} \qquad n=1, 2, 3, 4 \quad (5)$$

where n is the aperture and $C(i)$ is the contrast calculated as follows:

$$C(i) = \frac{p(i)_{flat} - p(i)_{obj}}{p(i)_{obj}} \quad (6)$$

where $p(i)_{flat}$ and $p(i)_{obj}$ are the mean values of the grey levels where the X-ray flux is not attenuated by the object and where the X-ray flux has been attenuated by the object, respectively, calculated on the image acquired using the aperture i.

2.6 Measurements

The axes of symmetry of the test objects were positioned along the rotational axis of the scanner. The distance from the rotation axis to the detector plane was set to 226 mm. The X-ray high voltage was set to 450 kVp and the current was set to 2 mA.

The measured projections were divided by the blank scan (i.e. image acquired without object being present). This procedure removes some of the geometric effects and scanner non-uniformities, such as the spatial irregularity of the source radiation [14]. To correct for the dark current of the CCD we acquired a dark image with the same exposure time as the experiment and we subtracted it from the measured image.

3. RESULTS AND DISCUSSION

3.1 Validation

Figure 4 shows profiles from simulated and measured projections of the step wedge and the aluminum box with copper rods. The measured projections were corrected for the non-uniformity of the scanner (blank scan correction) and for the dark current of the CCD. The simulated projections were divided by their blank scan image. The profiles obtained from the measurements and from the simulations are in good agreement. For the aluminum box the NE is below 1.5 % in correspondence to the Cu rods, and below 1 % in correspondence to the aluminum. For the step wedge the NE in correspondence to the steps of thickness up to 80 mm is below 1.5%; for the step 100 mm thick it is 5.9 %. The NE is higher in correspondence to the step 100 mm thick as a result of a low signal to noise ratio due to a stronger attenuation. The simulated profiles of the first-order scattering, second-order scattering and higher order scattering are also shown. We see clearly than the first-order scattering is the major component of the scattering for the objects considered. While the shape of the profile of the first-order scattering strongly depends on the shape of the object, the profiles of the second and higher order scattering are almost constant.

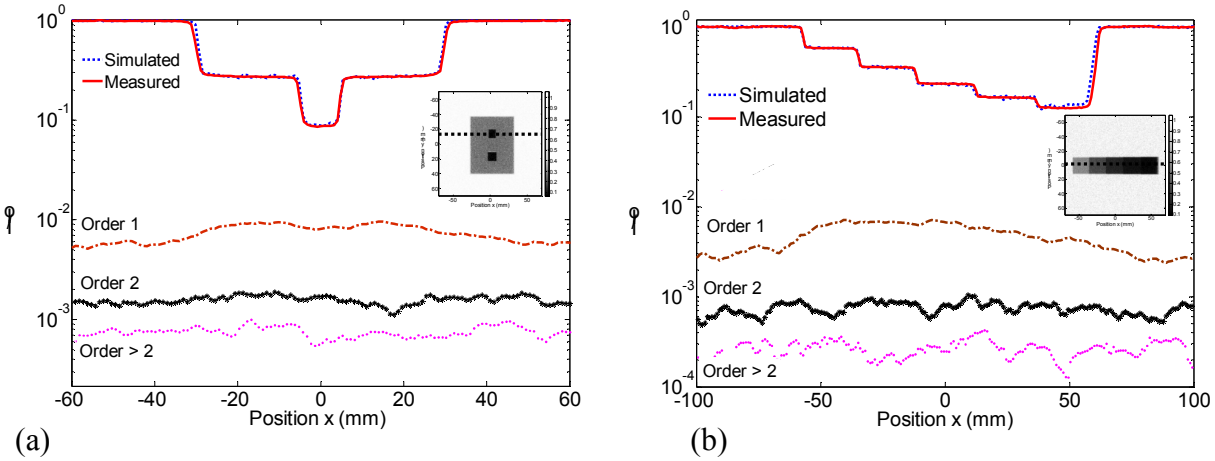

Figure 4. (a) Profiles of the Al box with Cu rods extracted from the simulated and measured images. The simulated profiles of the 1st order scattering, 2nd order scattering, and higher order scattering are also plotted. (b) The same for the step wedge.

3.2 Scatter characterization

Figure 5 shows the simulated profiles of the primary radiation, primary plus scattered radiation (total), first, second, and higher order scattering of the hollow cylinders. The values of the SPR_1, SPR_2, and $SPR_{>2}$ for the investigated cylinders are listed in table 1. For the hollow cylinder of diameter 75 mm the maximum value of the SPR_1 was estimated to be below 4 %, the SPR_2 and $SPR_{>2}$ below 1 %. In the hollow cylinder of 100 mm diameter the maximum value of SPR_1 rises to 10 %, SPR_2 and $SPR_{>2}$ are below 3 %. For the hollow cylinder of 150 mm diameter the SPR_1 becomes 40 %, the SPR_2 is about 20 %, and the $SPR_{>2}$ is around 30 %. In the hollow cylinder of diameter 200 mm the SPR_1 reaches a maximum value of about 70 %, the SPR_2 is lightly below 50 %, and the $SPR_{>2}$ is about 120 %. For the cylinders of diameter larger than 100 mm, the contribution of the second and higher order scattering should therefore be taken into account to increase the accuracy of the simulated image and to correct for the scatter in the scatter correction algorithms.

Table 2 presents the values of the contrast calculated from the profile of the primary ($C_{Primary}$) and primary plus scattered radiation (C_{Total}). The values of the ratio between $C_{Primary}$ and C_{Total} are also listed. It is interesting to notice that the value of C_{Total} is very close to $C_{Primary}$ in case of cylinders of diameters up to 100 mm, whereas, for the large cylinder of diameter 200 mm C_{Total} is approximately 0.5 times $C_{Primary}$.

Table 1. Scatter-to-primary ratio (SPR) of the 1st order scattering, 2nd order scattering, and higher than 2nd for the cylindrical objects. The values were calculated from the central line in two positions: the centre of the cylinder and the region of maximum path length.

Diameter (mm)	SPR_1%		SPR_2%		$SPR_{>2}$ %	
	center	max	center	max	center	max
75	1.9 ± 0.02	3.7 ± 0.2	0.222 ± 0.003	0.50 ± 0.02	0.138 ± 0.008	0.32 ± 0.01
100	4.4 ± 0.1	10.4 ± 0.2	0.96 ± 0.02	2.63 ± 0.06	1.06 ± 0.02	2.83 ± 0.07
150	12.8 ± 0.3	40 ± 2	5.8 ± 0.2	18.2 ± 0.9	10.8 ± 0.3	33 ± 2
200	31 ± 3	72.2 ± 0.8	18 ± 2	45.4 ± 0.5	46 ± 4	116 ± 1

Table 2. Values of contrast calculated from the primary radiation, $C_{primary}$, primary plus scattered radiation, C_{total}, and ratio between $C_{primary}$ and C_{total}.

Diameter (mm)	$C_{Primary}$	C_{Total}	$C_{Primaryl}$/ C_{Total}
75	1.24 ± 0.04	1.20 ± 0.04	1.03
100	3.9 ± 0.1	3.7 ± 0.1	1.05
150	21.3 ± 0.7	16.5 ± 0.5	1.30
200	94 ± 9	48 ± 2	1.96

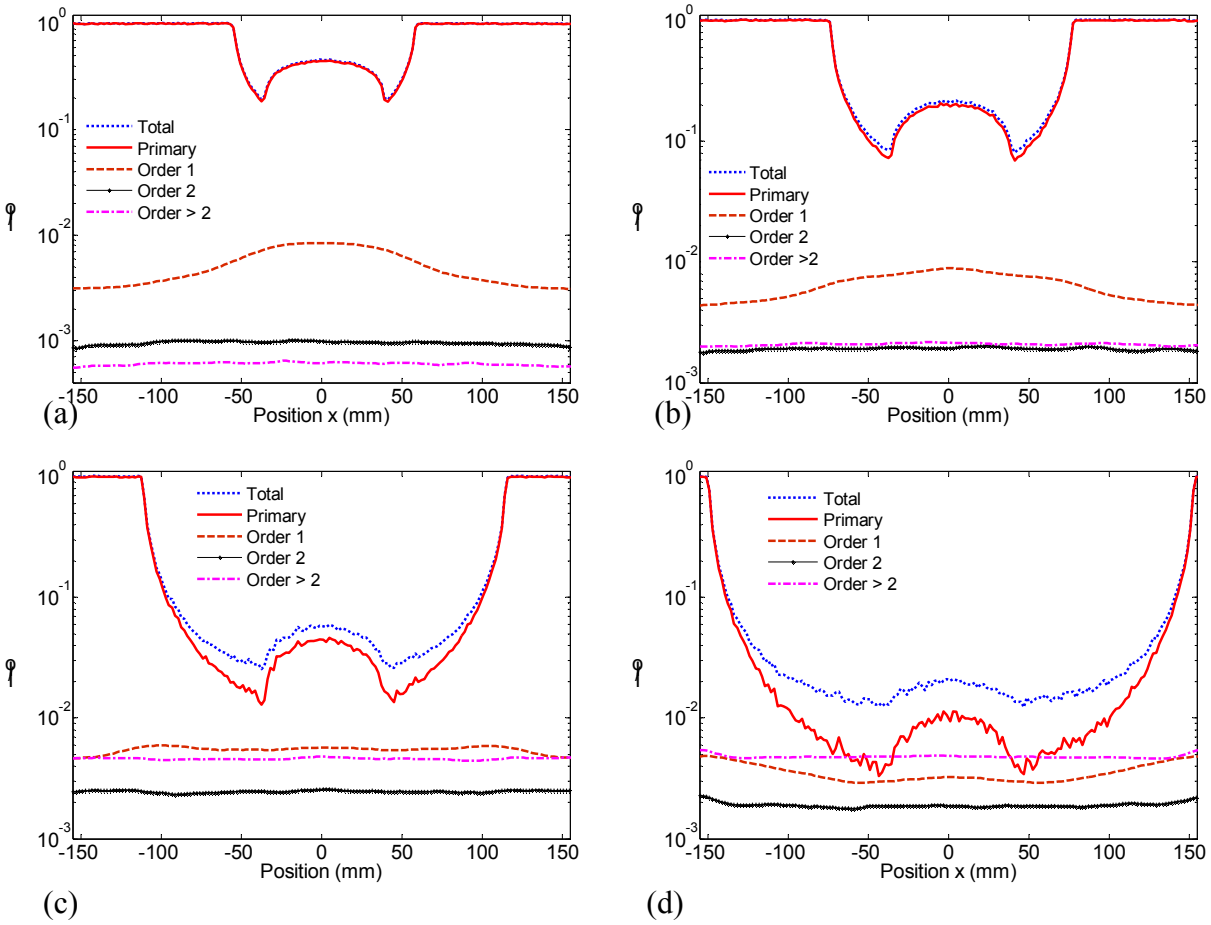

Figure 5. (a) Profiles of the primary, total, 1st order scattering, 2nd order scattering, and higher order scattering for the hollow Al cylinder of diameter 75 mm. (b) The same for the hollow cylinder of diameter 100 mm. (c) The same for the hollow cylinder of diameter 150 mm. (d) The same for the hollow cylinder of diameter 200 mm. The source-object distance was set to 1000 mm and the pixel size to 1.92 x 1.92 mm^2. The filter of 1.0 mm of silver was not simulated.

3.3 Scatter background

We performed some experiments to evaluate the degradation of the contrast due to the scatter background. Figure 6 shows the profiles of the aluminum box along the central axis of the detector. We see clearly that the underestimation of the attenuation increases as the aperture of the X-ray beam (i.e. the background scatter) increases. The value of the degradation of the contrast defined by the equation (5) calculated from the profiles is 1.22 in case of aperture 2, 1.43 of aperture 3 and 1.59 of aperture 4. We conclude that the scatter background reduces significantly the contrast and should be reduced by using X-ray source collimators.

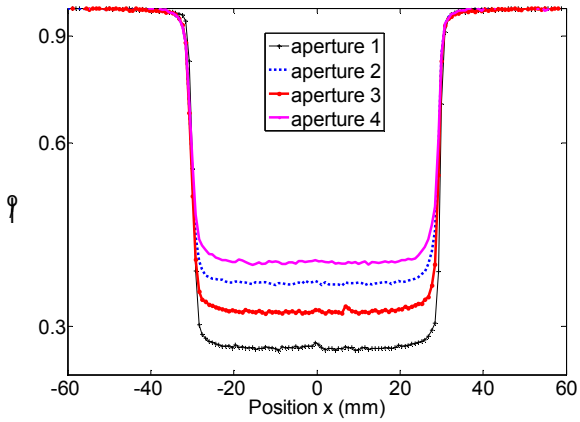

Figure 6. Profiles of the Al box corresponding to the horizontal central line of the detector acquired using different X-ray beam apertures.

4. CONCLUSIONS

A MC simulation using the code GEANT4 has been developed and validated to evaluate the contribution of the scatter of a CT system equipped with an X-ray tube of 450 kV and an area detector. The images formed by the first, second and higher order scattering were simulated for several hollow aluminum cylinders. For the cylinders of diameter up to 100 mm the scatter-to primary ratio of second and higher order scattering is below 1 % and 3 %, respectively, for the cylinder of diameter 150 mm it is 18 % and 33%, and for the cylinder of diameter 200 mm it is 45 % and 120 %. Therefore, it is necessary to consider also the multiple scattering to optimize cone beam CT systems for industrial applications. Unless strongly collimated, the scatter background has been found to decrease considerably the contrast of the image.

ACKNOWLEDGMENTS

This research was supported by the Swiss State Secretariat for Education and Research and the European Commission within the sixth framework project DETECT (New product design and engineering technologies based on next generation computed tomography).

REFERENCES

[1] Evans, R.D., *The atomic nucleus*. 1955, New York: McGraw-Hill.

[2] Glover, G.H., *Compton Scatter Effects in Ct Reconstructions.* Medical Physics, 1982. **9**(6): p. 860-867.

[3] Joseph, P.M. and R.D. Spital, *The Effects of Scatter in X-Ray Computed-Tomography.* Medical Physics, 1982. **9**(4): p. 464-472.

[4] Kyriakou, Y., T. Riedel, and W.A. Kalender, *Combining deterministic and Monte Carlo calculations for fast estimation of scatter intensities in CT.* Physics in Medicine and Biology, 2006. **51**(18): p. 4567-4586.

[5] Boone, J.M. and J.A. Seibert, *An Analytical Model of the Scattered Radiation Distribution in Diagnostic-Radiology.* Medical Physics, 1988. **15**(5): p. 721-725.

[6] Chan, H.P. and K. Doi, *The Validity of Monte-Carlo Simulation in Studies of Scattered Radiation in Diagnostic-Radiology.* Physics in Medicine and Biology, 1983. **28**(2): p. 109-129.

[7] Endo, M., et al., *Effect of scattered radiation on image noise in cone beam CT.* Medical Physics, 2001. **28**(4): p. 469-474.

[8] Kalender, W., *Monte-Carlo Calculations of X-Ray Scatter Data for Diagnostic-Radiology.* Physics in Medicine and Biology, 1981. **26**(5): p. 835-849.

[9] Colijn, A.P. and F.J. Beekman, *Accelerated simulation of cone beam X-ray scatter projections.* Ieee Transactions on Medical Imaging, 2004. **23**(5): p. 584-590.

[10] Agostinelli, S., et al., *GEANT4-a simulation toolkit.* Nuclear Instruments & Methods in Physics Research Section a-Accelerators Spectrometers Detectors and Associated Equipment, 2003. **506**(3): p. 250-303.

[11] Allison, J., et al., *Geant4 developments and applications.* Ieee Transactions on Nuclear Science, 2006. **53**(1): p. 270-278.

[12] Apostolakis, J., et al., *GEANT4 Low energy electromagnetic models for electrons and photons.* INFN/AE-99/18, 1999.

[13] Miceli, A., et al., *Comparison of simulated and measured spectra of an industrial 450 kV X-ray tube.* Nuclear Instruments & Methods in Physics Research Section A, 2007. **580**(1): p. 123-126.

[14] Colijn, A.P., et al., *Experimental validation of a rapid Monte Carlo based micro-CT simulator.* Physics in Medicine and Biology, 2004. **49**(18): p. 4321-4333.

Corresponding author.
Tel.: +41448234336; fax: +41448234579. E-mail address: alice.miceli@empa.ch